A Machine Learning System for Precipitation Estimation Using Satellite and Ground Radar Network Observations

Article *in* IEEE Transactions on Geoscience and Remote Sensing · October 2019

DOI: 10.1109/TGRS.2019.2942280

4 authors, including:

Haonan Chen
Colorado State University
107 PUBLICATIONS **747** CITATIONS

SEE PROFILE

Robert Cifelli
National Oceanic and Atmospheric Administration
125 PUBLICATIONS **3,176** CITATIONS

SEE PROFILE

A Machine Learning System for Precipitation Estimation Using Satellite and Ground Radar Network Observations

Haonan Chen, *Member, IEEE*, V. Chandrasekar, *Fellow, IEEE*, Robert Cifelli, and Pingping Xie

***Abstract*— Space-based precipitation products are often used for regional and/or global hydrologic modeling and climate studies. A number of precipitation products at multiple space and time scales have been developed based on satellite observations. However, their accuracy is limited due to the restrictions on spatiotemporal sampling of the satellite sensors and the applied parametric retrieval algorithms. Similarly, a ground-based weather radar is widely used for quantitative precipitation estimation (QPE), especially after the implementation of dual-polarization capability and urban scale deployment of high-resolution X-band radar networks. Ground-based radars are often used for the validation of various spaceborne measurements and products. This article introduces a novel machine learning-based data fusion framework to improve the satellite-based precipitation retrievals by incorporating dual-polarization measurements from a ground radar network. The prototype architecture of this fusion system is detailed. In particular, a deep learning multi-layer perceptron (MLP) model is designed to produce the rainfall estimates using the geostationary satellite infrared (IR) data and low earth orbit satellite passive microwave (PMW)-based retrievals as inputs. The high-quality rainfall products from the ground radar network are used as the target labels to train this MLP model. An urban scale demonstration study over the Dallas–Fort Worth (DFW) metroplex is presented. In addition, the Climate Prediction Center morphing technique (i.e., CMORPH) is adopted for preprocessing of the satellite observations. Rainfall products from this deep learning system are evaluated using the standard CMORPH products. The results show that the proposed data fusion framework can be used for generating accurate precipitation estimates and could be considered as an alternative tool for developing future satellite retrieval algorithms.**

Manuscript received May 9, 2019; revised July 22, 2019; accepted September 16, 2019. Date of publication October 7, 2019; date of current version January 21, 2020. This work was supported in part by the National Science Foundation (NSF) Hazards SEES Program, in part by the NASA Global Precipitation Measurement (GPM)/Precipitation Measurement Mission (PMM) Program, and in part by the Physical Sciences Division (PSD), NOAA's Earth System Research Laboratory (ESRL). *(Corresponding author: Haonan Chen.)*

H. Chen is with the Physical Sciences Division (PSD), National Oceanic and Atmospheric Administration (NOAA)'s Earth System Research Laboratory, Boulder, CO 80305 USA, and also with the Cooperative Institute for Research in the Atmosphere (CIRA), Fort Collins, CO 80523 USA (e-mail: haonan.chen@noaa.gov).

V. Chandrasekar is with the Department of Electrical and Computer Engineering, Colorado State University, Fort Collins, CO 80523 USA.

R. Cifelli is with the Physical Sciences Division (PSD), National Oceanic and Atmospheric Administration (NOAA)'s Earth System Research Laboratory, Boulder, CO 80305 USA.

P. Xie is with the National Oceanic and Atmospheric Administration (NOAA)' Climate Prediction Center, College Park, MD 20740 USA.

Color versions of one or more of the figures in this article are available online at http://ieeexplore.ieee.org.

Digital Object Identifier 10.1109/TGRS.2019.2942280

***Index Terms*— CMORPH, Dallas–Fort Worth (DFW), deep learning, dual polarization, quantitative precipitation estimation (QPE), radar network, satellite observations.**

I. Introduction

PRECIPITATION plays a key role in understanding the global, continental, and regional water cycles. Accurate precipitation measurements or estimates are vital in various climate, hydrologic, and weather forecast models. Therefore, a large infrastructure has been built around the world over a period of time to measure precipitation and its space–time distributions. Typical instruments include rain gauges that can directly measure rainfall, and remote sensors, such as weather radars and satellites, can indirectly estimate precipitation.

Rain gauges have traditionally been used for precipitation estimation. However, a large number of rain gauges must be deployed in order to capture the complex spatial variabilities of precipitation since gauges only provide pointwise measurements. In the real world, this is neither possible nor necessary due to the arduous nature of deployment and maintenance. A recent study by Kidd *et al.* [1] concluded that the total area measured globally by all currently available rain gauges was surprisingly small, equivalent to less than half a football field.

Compared with rain gauges, satellites have better coverage over the globe, especially over the ocean and polar regions. A number of quasi-global satellite precipitation products at different temporal and spatial resolutions have been developed in recent years, including the precipitation estimation from remotely sensed information using artificial neural network (PERSIANN) and its improved versions [2]–[4], the Tropical Rainfall Measuring Mission (TRMM) Multisatellite Precipitation Analysis (TMPA) [5], the Global Satellite Mapping of Precipitation (GSMaP) [6], [7], the Climate Prediction Center (CPC) MORPHing technique (CMORPH) [8], [9], and the recent Integrated Multi-satellitE Retrievals for Global Precipitation Measurement (IMERG) [10]. These satellite-based precipitation products are commonly used for natural disaster monitoring worldwide and for initializing large-scale numerical weather prediction models and evaluating the model-based precipitation forecasts (see [11], [12]).

Different satellite precipitation products are derived using different techniques. However, all satellite-based products are essentially derived using either geostationary (GEO) satellite infrared (IR) data or passive microwave (PMW) measurements from low earth orbit (LEO) satellite sensors or a combination

of both. The IR-based algorithms estimate the rain rates based on cloud-top brightness temperatures [13]. In general, a lower temperature will be associated with more precipitation. Such algorithms are adequate for convective rainfall, but not for stratiform or warm-top rainfall [14]. Compared with IR methods, the PMW-based retrievals have better physics, that is, at low-frequency bands, PMW sensors are able to sense the thermal emission of raindrops, whereas at high-frequency bands, the PMW sensors can detect scattering properties of ice particles in the precipitation layer and on tops of convective systems [15], [16]. IR data and PMW measurements are often combined to derive improved precipitation products. For example, the CMORPH product takes advantage of the high temporal resolution of the GEO satellite IR imagery to create motion vectors of the cloud systems and subsequently applies the cloud motion vectors to the PMW-based retrievals to produce precipitation estimates over the whole globe [8], [9].

Although space-based precipitation products provide an excellent tool for large-scale hydrologic and climate studies as well as improved situational awareness for operational forecasts, their accuracy is restricted due to the limitations of spatial and temporal sampling and the implemented parametric retrieval algorithms [17], [18], particularly for light precipitation or extreme events such as heavy rain. On the other hand, ground-based weather radar has shown great advantages in conducting high-resolution precipitation observations over wide areas in a relatively short time span. In addition, polarization diversity has great potential to characterize precipitation microphysics through observing the internal structure of storms and associated raindrop size distributions [19]–[21]. Therefore, ground-based, dual-polarization radar systems are widely used in hydrometeorological applications, and they serve as cornerstones of the national severe weather forecast and warning infrastructure in many countries. Recently, the sensing capabilities of the U.S. National S-band Weather Radar Network were further enhanced by the deployment of high-resolution short-wavelength (i.e., X-band) polarimetric gap-filling radars [22]–[25]. These X-band radars are developing their own operational domains for disaster detection and mitigation, especially in urban environments [25]–[27]. One of the successful examples is the research-to-operations radar network deployed in the Dallas–Fort Worth (DFW) metroplex by the National Science Foundation Engineering Research Center for Collaborative Adaptive Sensing of the Atmosphere (CASA) [23], [28], [29]. To date, the CASA DFW network has been operating for over seven years, providing real-time end-to-end weather information to weather forecasters, public safety officials, and other stakeholders in the DFW area.

Ground radar-based precipitation estimates are also widely used for the validation of various satellite products, especially instantaneous precipitation rates [30]–[35]. Ground radar systems are always key components in the ground validation activities of the National Aeronautics and Space Administration (NASA) Precipitation Measurement Missions (PMM). In addition, the ground radar-based precipitation estimates are often used as the references in deriving parametric algorithms for satellite precipitation retrievals. For example, the IR-based parametric rainfall algorithms can be obtained through nonlinear regression between the radar-derived precipitation rates and the collocated cloud-top brightness temperature information [13]. Nevertheless, most of these previous studies only used ground radar products as independent sources for verifying satellite products (see [31], [34], [36]–[38]). In addition, almost all the satellite-based rainfall algorithms derived with the aid of radar rainfall estimates are in simple parametric forms [39]. Very few studies have focused on combining ground radar and satellite precipitation measurements for improved precipitation estimation. The more sophisticated nonparametric approaches are rarely used in regard to this matter. To this end, this article introduces an innovative machine learning-based mechanism to improve spaceborne precipitation retrievals by incorporating dual-polarization measurements from a ground-based radar network.

This article is also motivated by the rapid development of deep learning approaches that have been successfully implemented in many applications [40]. In particular, a multi-layer perceptron (MLP) system is designed using the PMW and IR data as inputs and the ground radar-derived precipitation products as target labels to train the MLP model. In Section II, the generic machine learning system for radar and satellite precipitation data fusion is described, and the design and optimization of the proposed MLP model will be detailed. Section III presents an urban scale application of the proposed machine learning approach over the DFW metroplex. Section IV summarizes the main findings of this study and suggests the directions for future research.

II. MLP Model for Radar and Satellite Precipitation Data Fusion

Since McCulloch and Pitts [41] developed the first conceptual model of an artificial neural network, its application has expanded tremendously over the past few decades. Nowadays, deep neural network (or deep learning) is one of the most commonly used approaches to machine learning. Therefore, we consider a deep learning approach in building the machine learning system for radar and satellite precipitation data fusion. It should be noted that there may be other machine learning approaches that are also suitable for this topic, including inductive logic programming and Bayesian networks, among others. Finding such approaches is beyond the scope of this article.

A. System Design

A deep neural network is generally modeled as the collection of neurons that are connected in an acyclic graph [40]. It is often organized into distinct layers of neurons. As the fundamental element of a neural network, the artificial neuron is also referred to as "perceptron," which takes several inputs and produces a single output. For a single perceptron that has n inputs, a simple rule for computing the output is to assign different weights $w_1, w_2, \ldots, w_n$ to each input according to the importance of the respective inputs to the output. The perceptron's output y is determined by the weighted sum $y = f(\sum_i^n w_i x_i + b)$, where x_i is the input element, w_i is the

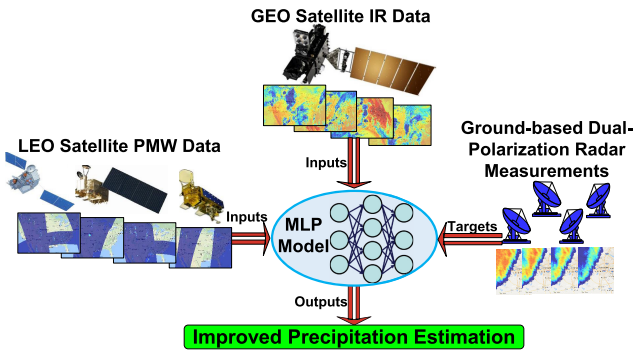

Fig. 1. Conceptual diagram of a machine learning system for radar and satellite precipitation data fusion. Essentially, the system is trained to produce rainfall estimates based on satellite observations/retrievals using ground radar observations/estimates as training targets.

weight corresponding to input x_i, b is an error term, and $f(*)$ is the activation function. In this article, the rectified linear unit (ReLU) $f(x) = \max(0, x)$ is employed as the activation function as it has strong biological and mathematical justifications [42], [43]. In fact, the ReLU is the most commonly used activation function in deep learning models today [44]. Fig. 1 shows a conceptual diagram of the machine learning system designed for satellite and radar precipitation estimation. In short, the inputs include IR and PMW measurements from multiple satellite sensors. The outputs are estimated precipitation rates, and the ground-based radar observations serve as training targets. The core part of this machine learning system is an MLP model that ingests radar and satellite data and produces the corresponding precipitation estimates.

In this article, we use the same inputs as CMORPH, which include the PMW-based precipitation retrievals and IR brightness temperature information. In particular, the IR data are extracted from five GEO satellites, including Himawari-8 operated by the Japan Meteorological Agency, GOES-West and GOES-East operated by the National Oceanic and Atmospheric Administration (NOAA), and Meteosat-7 and Meteosat-10 operated by the European Organisation for the Exploitation of Meteorological Satellites (EUMETSAT). The PMW-based precipitation retrievals are from a number of LEO satellites, including NOAA polar-orbiting operational meteorological satellites (NOAA-15, NOAA-16, NOAA-17, NOAA-18, and NOAA-19), polar-orbiting meteorological satellites (MetOp-A and MetOp-B) developed by the European Space Agency, the U.S. Defense Meteorological Satellite Program (DMSP) satellites (DMSP-13, DMSP-14, DMSP-15, DMSP-16, DMSP-17, and DMSP-18), the second generation of Chinese polar-orbiting meteorological satellite (FY-3B), and NASA's TRMM and Aqua satellites. The satellite measurements are examined by the CMORPH developers at NOAA/CPC [9] before ingested into the deep learning model. In addition, we adopt the CMORPH rainfall mapping technique to combine the data from individual satellites to latitude and longitude grids on a global scale [8]. In particular, the combined IR data are produced on 4 km $\times$ 4 km grids every 30 min, while the combined PMW-based retrievals are generated on 8 km $\times$ 8 km grids at the same temporal resolution. A brief review of the CMORPH rainfall mapping technique is given in Section III-B. For more details, interested readers are referred to [8]. Here, it should be noted that the proposed deep learning model is not limited to the satellite data used by CMORPH. Measurements from other or future satellites (some of them are used in the newer version of CMORPH [9]) can be integrated in a straightforward manner.

The combined IR data and PMW-based retrievals then serve as key inputs to the deep learning MLP model for precipitation estimation. Fig. 2 shows the detailed architecture of this data fusion system, including an input layer, three hidden layers, and an output layer. In particular, three, nine, and three perceptrons are devised for the first, second, and third hidden layer, respectively. The determination of hyperparameters, such as the number of hidden layers and the number of perceptrons for each layer, will be discussed in Section II-B.

The system equation of the model shown in Fig. 2 can be expressed in the following form:

$$\mathbf{y_1} = f(\mathbf{w_1 x} + \mathbf{b_1}) \tag{1a}$$

$$\mathbf{y_2} = f(\mathbf{w_2 y_1} + \mathbf{b_2}) \tag{1b}$$

$$\mathbf{y_3} = f(\mathbf{w_3 y_2} + \mathbf{b_3}) \tag{1c}$$

$$\mathbf{z} = f(\mathbf{w_4 y_3} + \mathbf{b_4}) \tag{1d}$$

where $\mathbf{x} = [x_1, t_{\mathrm{PMW}}, x_2, t_{\mathrm{IR}}]$ is the input vector consisting of available PMW-based retrievals (x_1) and corresponding time (t_{PMW}), and IR observations (x_2) and corresponding observation time (t_{IR}); $\mathbf{y_1}$–$\mathbf{y_3}$ are the outputs of three hidden layers from left to right; $\mathbf{w_1}$–$\mathbf{w_4}$ are the weight vectors at the input layer and three hidden layers, respectively; $\mathbf{b_1}$–$\mathbf{b_4}$ are the bias terms associated with the input layer and three hidden layers, respectively; and $\mathbf{z}$ is the output of estimated rainfall, which will be compared with ground radar-based estimates.

Given the temporal resolution of combined satellite data (see the details in Section III-B), the model is trained and applied for each half-hour window. At each half-hour window, the availability of IR data is almost guaranteed at a given location. In contrast to the IR, the PMW-based retrievals are severely limited due to the spatial and temporal sampling natures of LEO satellites. Previous studies have concluded that PMW sensors could not cover most of the globe unless the data are composited for 3 h or longer period [8]. When the PMW-based retrievals are not available during a half-hour window, CMORPH computes the cross correlation between the consecutive IR images and propagates adjacent/available PMW-based retrievals using the derived correlations to obtain the estimates for the current time frame ($t = 0$ h) [8], [9]. In this article, we also use available PMW-based retrievals for time frames when there are no PMW sensor coverages. However, instead of propagating the existing PMW-based retrievals using IR-based motion vectors, the proposed deep learning model directly uses the existing PMW-based estimates. At the same time, the time difference between the available retrievals and the current time frame is considered an additional input to the model. Similar to CMORPH, a 3-h period is considered in this study when finding available PMW-based retrievals, that is, at any time (e.g., $t = 0$ h) when the PMW-based retrievals are not available, three frames before (i.e., $t - 1.5$, $t - 1$, and $t - 0.5$ h) and three frames after (i.e., $t + 0.5$, $t + 1$, and $t + 1.5$ h)

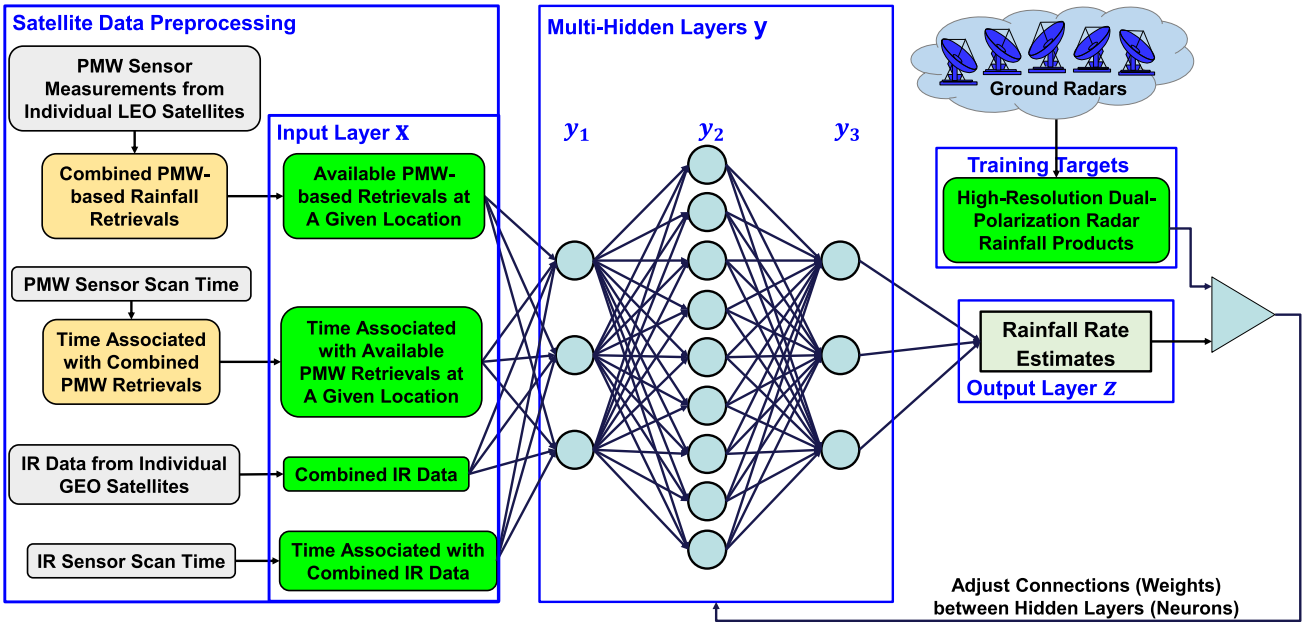

Fig. 2. Architecture of the deep learning model for satellite-based precipitation estimation using ground radar observations as references.

are considered. For example, at 02:00 UTC, if both IR data and PMW-based retrievals are available, x_1 and x_2 will be assigned as the PMW-based retrievals and IR data, respectively. Both t_{PMW} and t_{IR} will be current (i.e., $t_{\mathrm{PMW}} = 0$ h and $t_{\mathrm{IR}} = 0$ h). Otherwise, if the PMW-based retrievals are not available at 02:00 UTC, the model will use all available PMW data during 00:30-03:30 UTC. If PMW-based retrievals are available at 01:30 and 03:00 UTC, both will be used in x_1. Accordingly, t_{PMW} will be assigned as $t_{\mathrm{PMW}} = -0.5$ h and $t_{\mathrm{PMW}} = +1$ h for 01:30 and 03:00 UTC data, respectively. Occasionally, if there are no PMW measurements during a 3-h period, the closest data (i.e., only one frame) and the corresponding time difference will be used.

B. Model Selection and Optimization

As in many other machine learning problems, one cannot know the best values for model hyperparameters, including the number of hidden layers and learning rate. Essentially, the configuration of hyperparameters is external to the model and the hyperparameters cannot be estimated from input observables. They are usually fixed before the actual training process begins. As such, the determination of the deep learning MLP model hyperparameters for robust and accurate precipitation estimation for a given set of radar and satellite data partly relies on our experience and experiments. In this article, we use a grid search approach. As shown in Fig. 3(a), many hyperparameter candidates are predefined with different learning rates and numbers of hidden layer and associated perceptrons. The deep learning model is trained for each candidate pair to discover the one that results in the most accurate estimates. In the demonstration study (see Section III), it is found that the MLP model with three hidden layers that have respective three, nine, and three perceptrons will produce the best estimates (with sufficient accuracy compared with the current CMORPH product). This is also why such a configuration is used in Fig. 2. Nevertheless, it should be noted that such hyperparameter setting may need to be fine-tuned when more data are available or when this model is applied in different precipitation regimes.

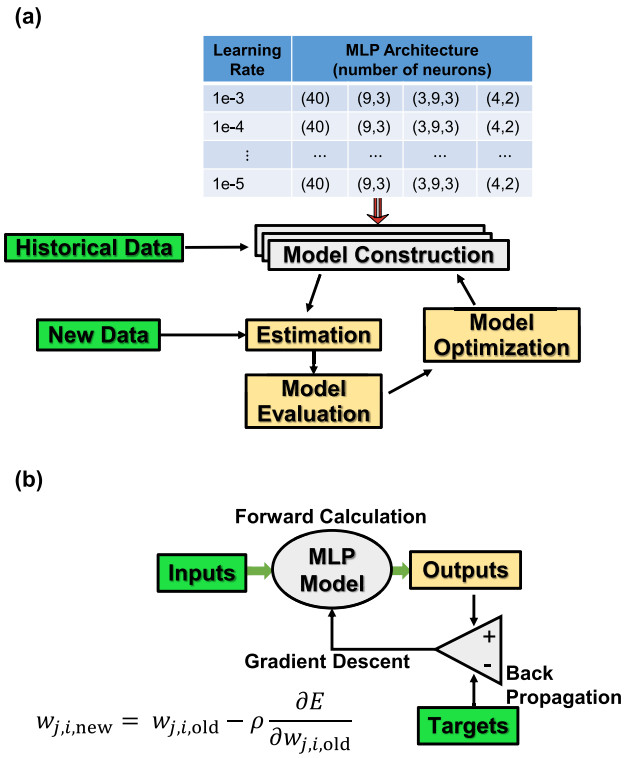

Fig. 3. Model selection and optimization. (a) Determination of model hyperparameters, including the numbers of hidden layers and perceptrons comprising each layer. The numbers in the parentheses refer to the number of hidden layers, whereas the values correspond to the number of nodes in each hidden layer. (b) Optimization of a given model using the gradient descent approach.

For the selected hyperparameters, the deep learning model is optimized using the gradient descent algorithm [45]. Fig. 3(b) shows the model training process to find the optimal solution. Essentially, the optimization procedure includes forward propagation for estimation and the backward propagation for error optimization (or changing weights). It is achieved through the following four steps.

1) *Forward Estimation:* Calculate the hidden layer outputs $\mathbf{y_i}$ and precipitation estimates $\mathbf{z}$ in (1) for given input satellite data $\mathbf{x}$.
2) *Compute Cost Function:* Calculate the mean square error E of $\mathbf{z}$ using target labels from ground radar measurements.
3) *Backward Propagation:* Compute the gradient $\partial E/\partial w_{i,j}$ of the cost function E.
4) *Gradient Descent:* Update weights $w_{i,j}$ using the gradient from step 3 until an optimal solution is reached.

In particular, the cost function is defined as the mean square error E of satellite rainfall retrievals with respect to ground radar rainfall estimates

$$E = \frac{1}{N}\sum (RR_R - RR_S)^2 \tag{2}$$

where RR_S represents the precipitation rate estimated using satellite data, RR_R is the training target label determined by ground radar network observations, and N is the total number of precipitation grids. The weights are updated based the following form:

$$w_{i,j\,(\text{new})} = w_{i,j\,(\text{old})} - \rho \frac{\partial E}{\partial w_{i,j\,(\text{old})}} \tag{3}$$

where ρ is the learning rate of the deep learning MLP model and $w_{i,j}$ is the weight associated with the jth node of the ith layer. The learning rate determines how quickly or slowly the model moves toward the optimal weights/solution. In applications, the learning rate should satisfy the condition of being less than $2/\lambda_{\min}$ to guarantee convergence to the point of local minimum [46]. Here, $\lambda_{\min}$ represents the minimum eigenvalue of the input covariance matrix. Based on our experiments, the learning rates listed in Fig. 3(a) can be adopted in the proposed deep learning model.

III. Urban Scale Demonstration in DFW Metroplex

The proposed MLP-based framework for radar and satellite data fusion is rather generic, requiring no restrictions on the implementation domain or particular type of ground- or space-based instrument. In other words, this model can be applied in any climate regions, provided that active radar and passive satellite measurements coexist. In this section, an urban scale demonstration study over the DFW metroplex is presented. The selection of this particular domain is also motivated by the development of a high-performance rainfall system for the dense CASA DFW radar network.

A. Ground Radar Rainfall System

The DFW network consists of eight high-resolution X-band radars and a standard National Weather Service (NWS) Next-Generation Weather Radar (NEXRAD) system operating at S-band [24]. All are working in the dual-polarization mode. Fig. 4 shows the layout of the DFW urban radar network. The 100-km range ring in red denotes the S-band NEXRAD, whereas the 40-km range rings in blue represent the coverage of eight polarimetric X-band radars. In particular, the area denoted by the grids shows the specific domain of this demonstration study. Both radar and satellite data are trimmed to match this 192 km × 200 km area when ingested into the proposed deep learning model.

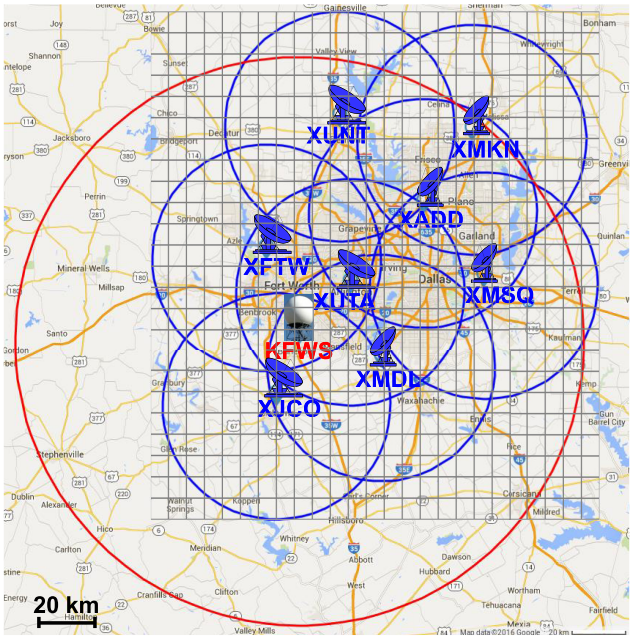

Fig. 4. Urban scale study domain for the proposed MLP-based precipitation estimation system. Circles in red (i.e., S-band) and blue (i.e., X-band) denote the layout of the DFW radar network. The letter symbols, such as "KFWS," correspond to the naming of various radars. The grids on top represent a 192 km × 200 km area, where this demonstration study will be focused on.

Chen and Chandrasekar [26] have developed a real-time high-quality rainfall system for the DFW radar network. In the following, a brief description of this urban radar quantitative precipitation estimation (QPE) system is provided. More details can be found in [24] and [26]. Fig. 5 shows the schematic of the DFW radar rainfall system, which takes advantage of the dual-polarization measurements that can be used to characterize precipitation microphysics. In particular, this QPE system consists of polarimetric radar rainfall algorithms for both S-band NEXRAD and X-band CASA radars. At S-band, a blended algorithm is implemented where the specific rainfall relations are guided by hydrometeor identification results [21], [47]. In this blended methodology, all the polarimetric measurements are used, including reflectivity Z_h, differential reflectivity Z_{dr}, specific differential phase K_{dp}, and correlation coefficient ρ_{hv}. The hydrometeor identification is determined via a region-based classification scheme that utilizes a vertical temperature profile with a series of thresholds and ranges of the polarimetric variables [48]. At X-band, only $R(K_{\text{dp}})$ is considered since $R(K_{\text{dp}})$ is the only estimator not affected by rain-path attenuation. In the DFW QPE system, K_{dp} fields from the synchronized observations of the eight X-band radars are merged to Cartesian grids first.

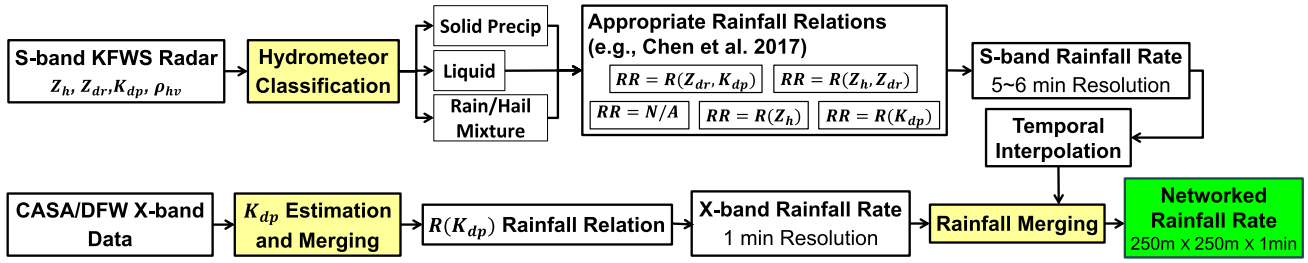

Fig. 5. Dual-polarization rainfall system for DFW urban radar network. Adapted from [26, Fig. 5].

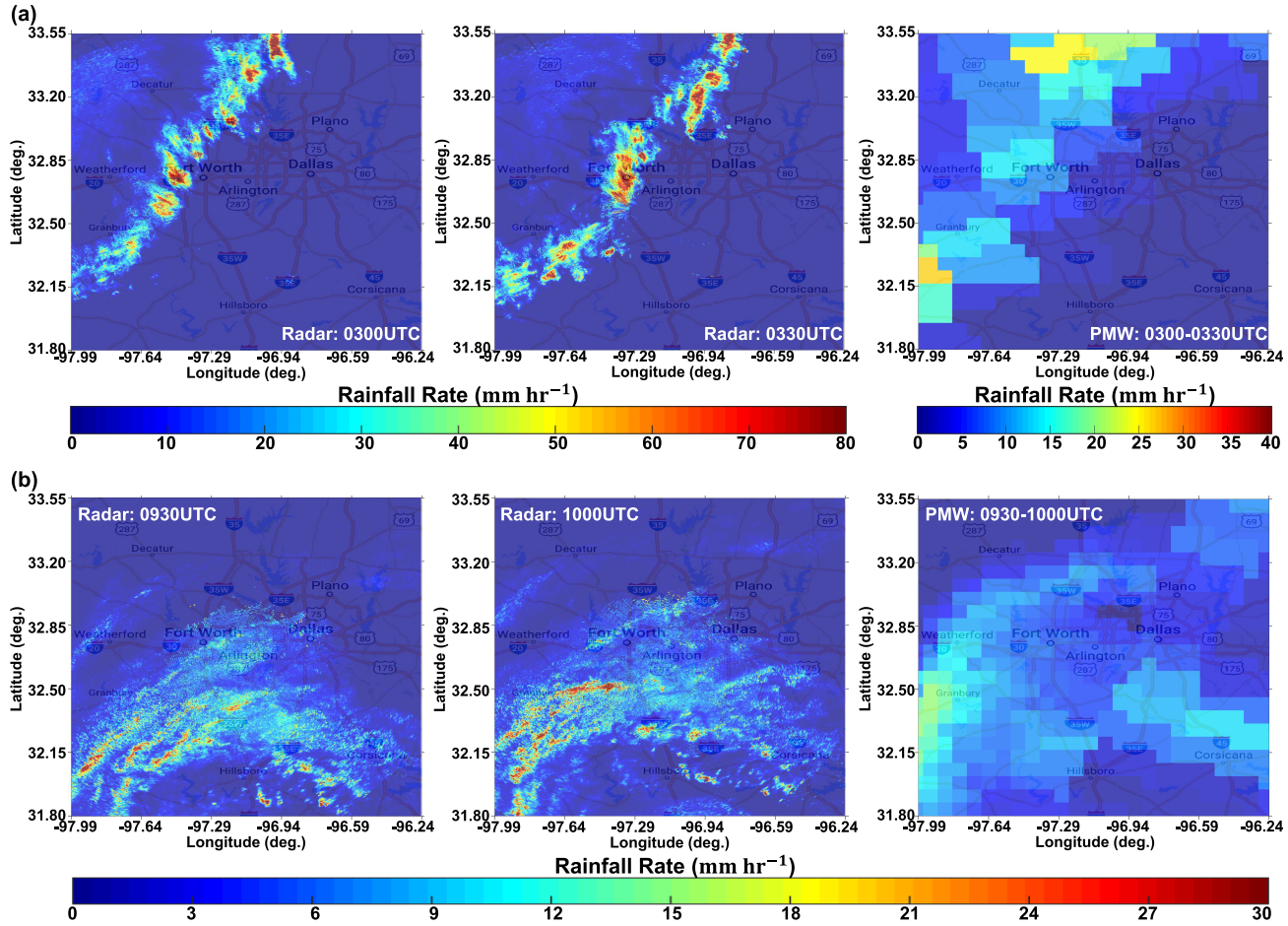

Fig. 6. Sample instantaneous rainfall rate products from the DFW urban radar network during (a) squall line event on May 29, 2015, and (b) widespread convective storm event on June 17, 2015. The two rain rate snapshots in (a) or (b) have a 30-min time difference, illustrating the storm change during a half-hour window. (Right) Rainfall retrievals from satellite-based PMW sensors during this half-hour window, which have much coarser resolution compared to ground radar-derived products.

Then, the $R(K_{\rm dp})$ relation is applied to the composite $K_{\rm dp}$ field to produce instantaneous rainfall rate estimates. In the composite process, the closer one the radar to a given grid pixel, the higher the priority that radar observation will have in the QPE. This is to ensure that the observations and estimates are close to the surface. Then, the S- and X-band estimates are combined to generate a network-level rainfall product. Overall, the DFW QPE system produces the real-time rainfall rate estimates at a spatial scale of 250 m $\times$ 250 m, and temporally, the instantaneous rain rates are updated every minute.

Fig. 6(a) shows the sample rainfall rate estimates from the DFW radar network during a squall line event on May 29, 2015, at 03:00 and 03:30 UTC. The two rain rate snapshots have a 30-min time difference, illustrating the storm change during a half-hour window. For comparison, the combined PMW-based precipitation retrievals during this half-hour window (03:00–03:30 UTC), which have much coarser resolution compared to the ground radar-derived products, are also shown in Fig. 6(a). Similarly, Fig. 6(b) shows the sample rainfall products during a widespread convective storm on June 17, 2015. Here, it should be noted that although the PMW-based retrievals are obtained every 30 min, they essentially represent the precipitation rates for an instantaneous observing time within a certain half-hour window, that is, the PMW-based retrievals on the right of Fig. 6(a) do not really correspond to an average of rainfall rate for 30 min (i.e., 03:00–03:30 UTC).

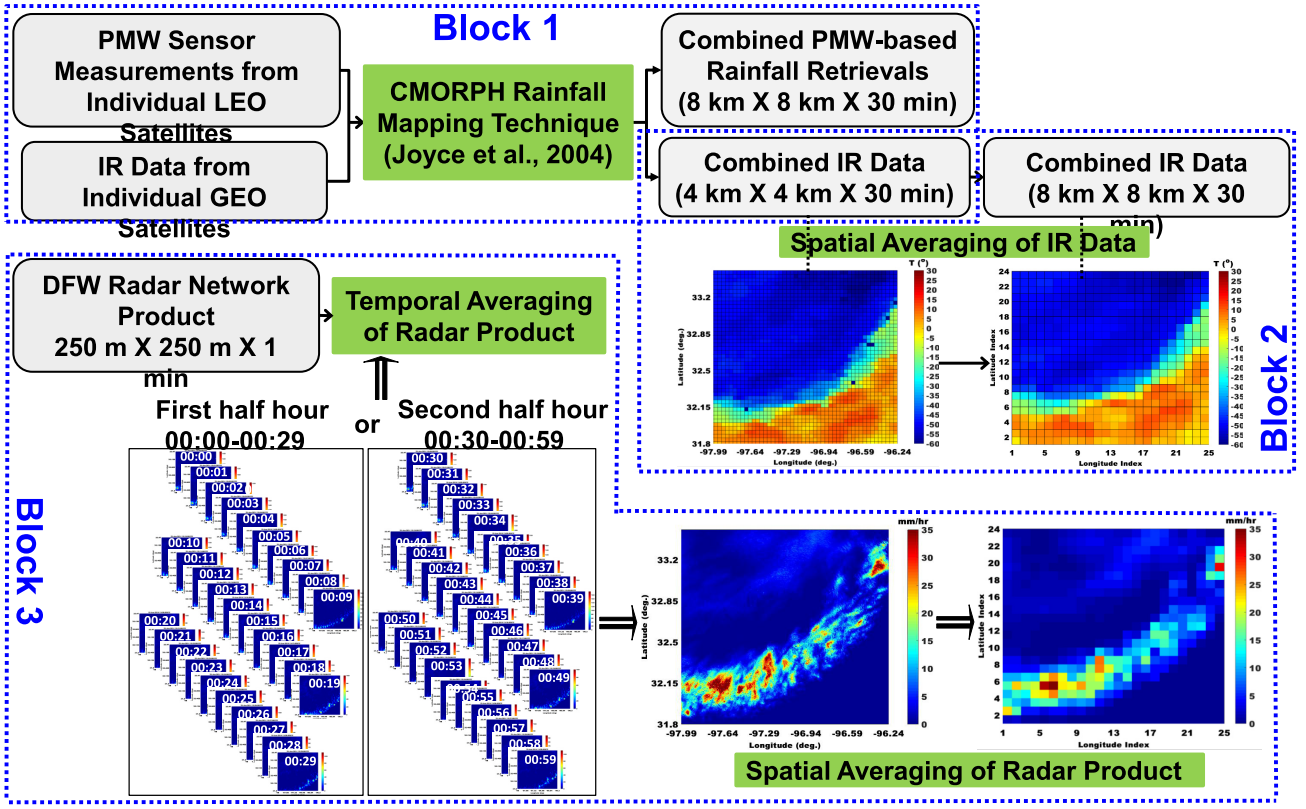

Fig. 7. Radar and satellite data preprocessing, including the spatial averaging of radar and satellite IR data, and temporal averaging of radar-based rainfall measurements. The preprocessed data will be ingested by the MLP model of the machine learning system in Fig. 2.

Rather, they are estimates for an instant between 03:00 and 03:30 UTC. This is partly why the storm location indicated by the PMW-based retrievals is somewhat different from that observed by the radar-based estimates in the left and middle of Fig. 6. This difference is not as significant during widespread precipitation events such as that shown in Fig. 6(b). The mismatching between different data sets should be resolved before ingesting them to the proposed deep learning MLP model. Radar and satellite data preprocessing with regard to this aspect will be detailed in Section III-B.

The DFW QPE system is very robust and has been continuously working for a number of years without any major incidents [24]. Quantitative comparison with a large number of local rain gauges shows that the DFW QPE system product has superior performance to both NEXRAD single- and dual-polarization rainfall products. The normalized standard error (NSE) of hourly rainfall rate is about 15%, demonstrating that the quality of the DFW product is among the best radar QPE results available in the literature (see [49]–[52]). The real-time QPE products from the DFW radar network are used by the local Weather Forecast Office and emergency managers operationally for issuing weather watches and warnings. The DFW rainfall products also serve as an input to the distributed hydrologic models for real-time flash flood predictions [53]. It is expected that the DFW radar rainfall data will be a good data set that can be used to validate various satellite-based precipitation estimates. In fact, previous studies have already used the high-resolution DFW rainfall products to validate and calibrate spaceborne dual-frequency precipitation radar (DPR) onboard the GPM satellite [32], [33], [54]. Therefore, we use this high-performance data set to conduct an urban scale demonstration study of the proposed deep learning model.

B. Data Preprocessing

As mentioned previously (see Section II-A), this article considers the observations from several GEO satellites and a number of LEO satellites. Each LEO satellite collects observations according to its own orbit, producing overpass measurements at different space–time resolutions. As a result, radar and satellite data preprocessing is necessary before executing the proposed deep learning model. Fig. 7 shows the preprocessing of radar and satellite data, including the temporal and spatial averaging of the high-resolution observations. In particular, the preprocessing includes the following steps.

First, we use the CMORPH mapping technique to combine individual satellite-based IR data and PMW-derived estimates (see Block 1 in Fig. 7). With regard to the IR data, the approach described in [55] is utilized to map each satellite IR image onto a rectilinear grid at 4 km $\times$ 4 km $\times$ 30 min resolution. The global IR data are then constructed by compositing IR window channel measurements from the five GEO satellites described in Section II-A. With regard to the PMW-based retrievals, the estimates from each satellite are first mapped to the nearest grid point on global rectilinear grids at 8 km $\times$ 8 km resolution (at the equator), which is determined by compromising the spatial resolution of various LEO satellite data sources [8]. Temporally, a half-hour interval is selected for PMW-based precipitation analyses in order to

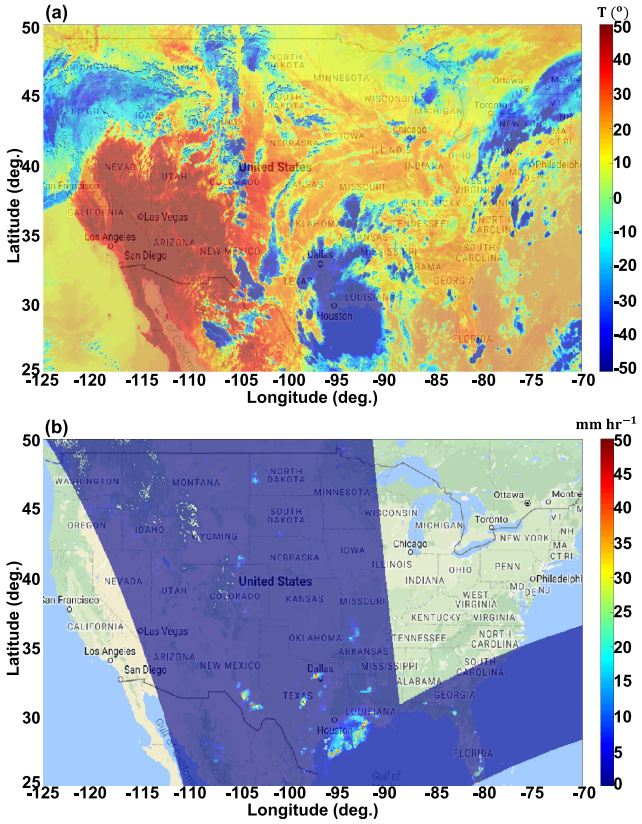

Fig. 8. Combined satellite data over the continental United States on June 25, 2014, at 20:00 UTC. (a) IR brightness temperatures mainly observed by GOES-West and GOES-East. (b) PMW-based rainfall retrievals.

match the resolution of IR data. If two or more estimates from the same satellite sensor are available for a given grid pixel, the average of rainfall estimates is calculated and used for that grid pixel. In reality, this only happens for high-resolution TRMM-based precipitation retrievals. In addition, at grid pixels within the satellite swath but with no rainfall estimates available, an inverse distance squared weighting interpolation of the nearest rainfall estimates is performed to create a spatially complete field within the overpass band [8]. For each half-hour window, after this process is done for all the individual satellites, precipitation retrievals from multiple satellites are combined according to the precedence of each sensor type [8], [9]. Fig. 8 shows the examples of combined IR brightness temperature data and PMW rain rates over the conterminous United States on June 25, 2014, at 20:00 UTC. It should be noted that although the global IR data are generated using five GEO satellites, the composite IR data used in the deep learning model are essentially from two satellites covering the continental United States (i.e., GOES-East and GOES-West).

Second, the spatial resolutions of ground radar-based rainfall estimates and the combined IR data are downscaled to match the coarse resolution of PMW-based retrievals (see Block 2 in Fig. 7). In particular, at each half-hour window, the combined IR brightness temperature data on 4 km $\times$ 4 km grids are spatially averaged to 8 km $\times$ 8 km resolution. The high-resolution (i.e., 250 m $\times$ 250 m) DFW radar rainfall products are also remapped on each 8 km $\times$ 8 km grid (see Block 3 in Fig. 7). Therein, 32×32 high-resolution radar grid pixels are linearly averaged to obtain rainfall estimates matching a single 8 km $\times$ 8 km grid. Temporally, 30 frames of DFW radar products (1-min resolution) from 00 to 29 min of each hour are averaged to obtain the estimates for the first half-hour window, and 30 frames from 30 to 59 min are averaged for the second half-hour window. The linear average is employed here only for simplicity's sake. More complicated and efficient interpolation approaches to rainfall data processing that can better reflect the rainfall pattern and distribution will be investigated in future studies. Overall, the spatiotemporal resolution of 8 km $\times$ 8 km $\times$ 30 min is used in the proposed deep learning MLP model.

In addition, both radar and satellite data are limited to the 192 km $\times$ 200 km area shown in Fig. 4. This area is densely covered by the X-band polarimetric radar network to ensure high quality of the target labels in the training process of the designed MLP model. As shown in Fig. 7, this particular domain includes 24 (latitude) $\times$ 25 (longitude) grid pixels of PMW-based precipitation retrieval at its composite resolution. The corresponding IR and ground radar data are processed on the same grids. Furthermore, as detailed in Section II-A, the PMW-based retrievals are not always available over this particular study domain due to the limited LEO satellite overpasses. Instead of using motion vectors derived from the IR data to propagate PMW-based retrievals (i.e., the CMORPH approach), this study only considers the available PMW data and the time difference between the available PMW rain rates and the IR data. To this end, a time tag is created for each available PMW frame during the preprocessing. The time tags, along with the IR data and available PMW-based retrievals, are used as key inputs to the MLP model. The preprocessed rainfall estimates from the DFW radar network are considered the target labels when training the MLP model.

C. Case Studies and Preliminary Results

In this demonstration study, 14 precipitation events that occurred in 2013, 2014, and 2015 are used in the analysis. Table I lists the dates of these precipitation events. Among the 14 events, 12 cases are utilized for training the designed deep learning MLP model, whereas the other two cases are used for testing purposes. Note that the separation of training and testing scenarios is rather random. In total, the training data set includes 960 h of data (i.e., 1920 half-hour frames). All the input data, including IR brightness temperature, PMW-based retrievals, as well as their associated time tags, are generated on 25×24 grids covering the DFW metroplex. The total number of training data pairs is about 1.15 million. The DFW radar network-based rainfall products are also generated for these 14 events. The products for the training events are used as target labels in the MLP model. After training the deep learning model for all hyperparameter candidates [see Fig. 3(a)], the trained (optimal) model is used to process the satellite data collected for the testing events to produce the estimated rainfall fields. The DFW radar products for the testing events are used to evaluate the trained model. The standard CMORPH products are also utilized to demonstrate the

TABLE I
TRAINING AND TESTING EVENTS FOR THE PROPOSED DEEP LEARNING SYSTEM

Precipitation Dates	Category
17-20 Apr 2013	Training
15-18 May 2013	Training
26-29 Oct 2013	Training
16-20 Jul 2014	Training
17-20 Mar 2015	Training
01-04 Apr 2015	Training
08-15 Apr 2015	Training
10-13 May 2015	Training
28-31 May 2015	Training
16-20 Jun 2015	Training
25-29 Nov 2015	Training
25-29 Dec 2015	Training
08-11 Jun 2013	Testing
23-27 Jun 2014	Testing

skill of the proposed deep learning precipitation data fusion system.

Fig. 9(a) shows the sample rainfall estimates with the trained MLP model using the satellite-based PMW and IR data collected for the validation event on June 24, 2014, at 23:00 UTC. For comparison, Fig. 9(b) and (c) shows the standard CMORPH products and the corresponding rainfall estimates from the ground-based DFW radar network, respectively. At this time frame, the combined PMW-based retrievals are available in this area and are similar to the CMORPH or MLP-based products. Similarly, Fig. 10 shows the results for another half-hour frame on June 25, 2014, at 19:00 UTC. The combined PMW-based retrievals are not available over the DFW region during this half-hour window, so both CMORPH and the proposed deep learning MLP model are using temporally surrounding observations to produce estimates for this time frame. Although there exist noticeable differences among the three estimates in Fig. 10(a)–(c), their overall patterns agree with each other fairly well. The results for other time frames or for the other validation event are not shown since essentially they show a similar performance. Such qualitative visual comparisons show that the proposed data fusion system is very promising in generating precipitation estimates, even for times when the PMW-based sensors provide no coverage.

In order to further demonstrate the performance of the proposed deep learning MLP model, the NSEs (NSE_{rain}) of precipitation estimates from this model and CMORPH system are computed for the products generated during the two validation events listed in Table I. Assuming the ground radar-based products (after averaging) as the ground truth, NSE_{rain} is defined as

$$\text{NSE}_{\text{rain}} = \frac{|E_R - R_R|}{R_R} \tag{4}$$

where E_R is the number of rainy pixels with rain rates above a given threshold from either CMORPH or the proposed deep learning model and R_R is the number of rainy pixels in the DFW radar network-based rainfall estimates. Here, R_R is independent of E_R since the ground radar estimates during the test scenarios are not used in the training process of the MLP model.

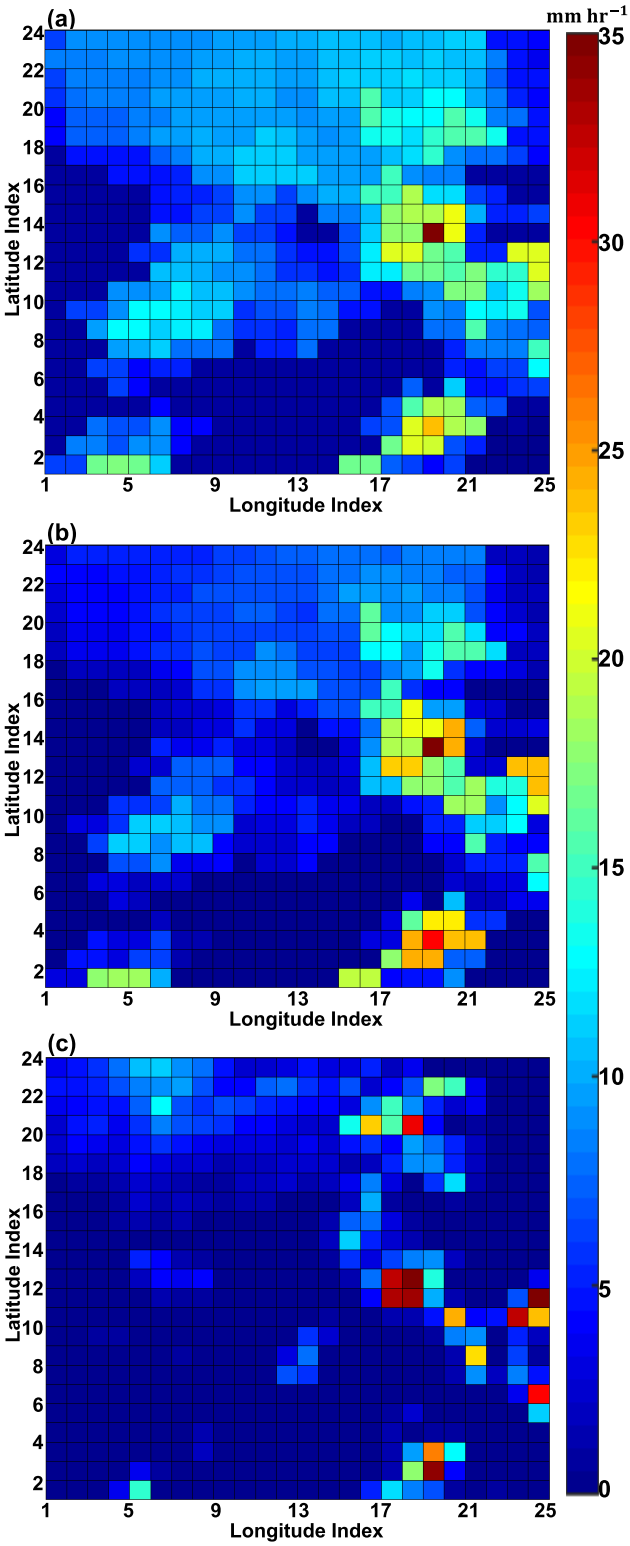

Fig. 9. Precipitation products on June 24, 2014, at 23:00 UTC. (a) Estimates from the proposed deep MLP model. (b) Standard CMORPH product. (c) Averaged rainfall estimates from the DFW radar network. At this time frame, the PMW-based retrievals are available, which are similar to the CMORPH or MLP-based products.

Table II shows the quantitative evaluation results based on all the estimates for these two test events. In particular, if a

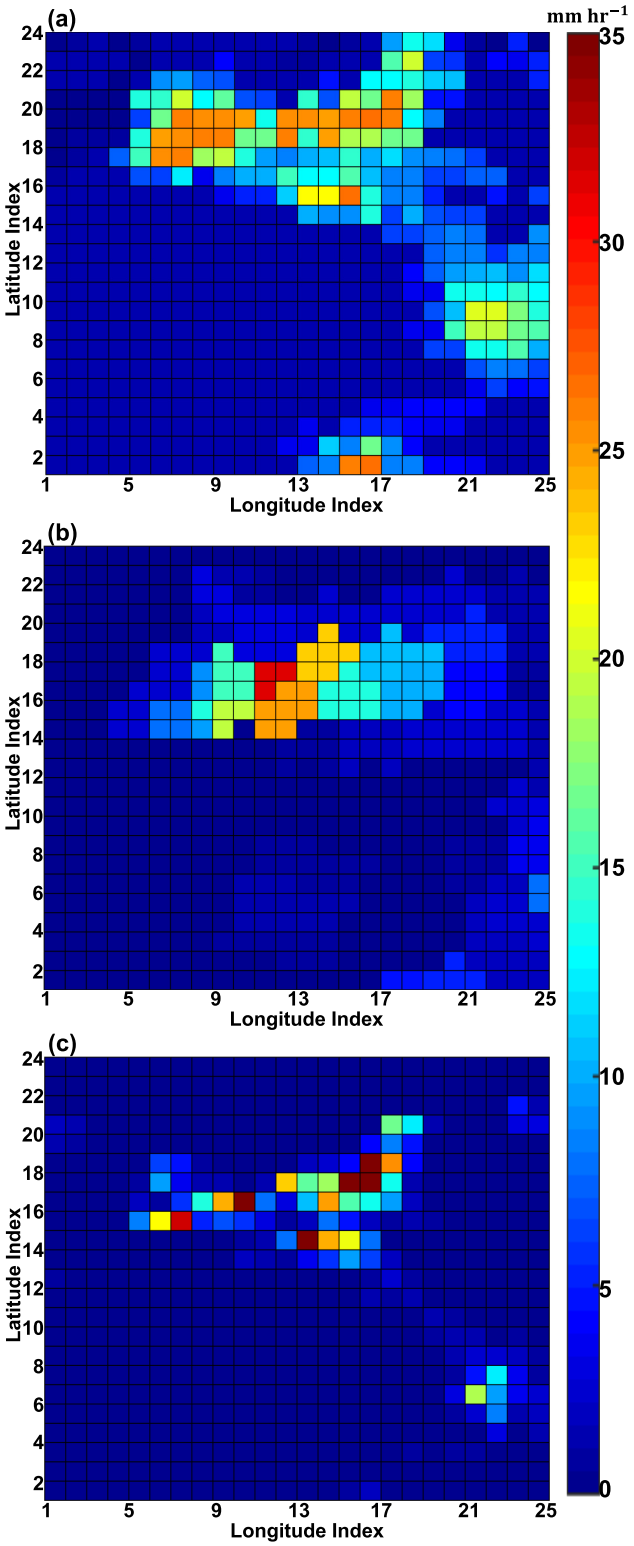

Fig. 10. Precipitation products on June 25, 2014 at 19:00 UTC. (a) Estimates from the proposed deep learning MLP model. (b) Standard CMORPH product. (c) Averaged rainfall estimates from the DFW radar network. At this time frame, the PMW-based retrievals are not available over the DFW area.

threshold of 0.5 mm h^{-1} is applied in the computation, NSE_{rain} of the MLP-based products is about 11%. When a higher threshold (i.e., 1 mm h^{-1}) is applied, the results become relatively worse since many grid pixels are reporting very light rain for most of the time frames during these two events. The CMORPH products have a similar performance, which again demonstrates the feasibility of the proposed MLP model in detecting rainfall. In addition, the probability distribution function (PDF) of rainfall rates estimated using different techniques is investigated. Fig. 11 shows the PDFs for rainfall products derived for the two validation events. Overall, they agree with each other very well, which further demonstrates the feasibility of the proposed system. It is also observed that this nonparametric machine learning approach can capture low rainfall rates, which is slightly better than CMORPH. Here, we also note that a more quantitative evaluation is challenging since the rainfall rates from ground radar represent an average over each half-hour window, whereas the PMW-based retrievals (inputs to the model) represent instantaneous rainfall rates sampled within a certain half-hour window. Such temporal mismatching may introduce additional errors in the quantitative evaluation analysis.

TABLE II

NSE OF RAINFALL ESTIMATES FROM THE PROPOSED DEEP LEARNING MLP MODEL AND THE STANDARD CMORPH SYSTEM. THE RESULTS SHOWN HERE ARE FOR THE TWO TESTING EVENTS LISTED IN TABLE I

	Normalized Standard Error (*NSE*)	
Threshold (mm hr^{-1})	CMORPH	Deep learning Model
0.5	15%	11%
1.0	40%	37%

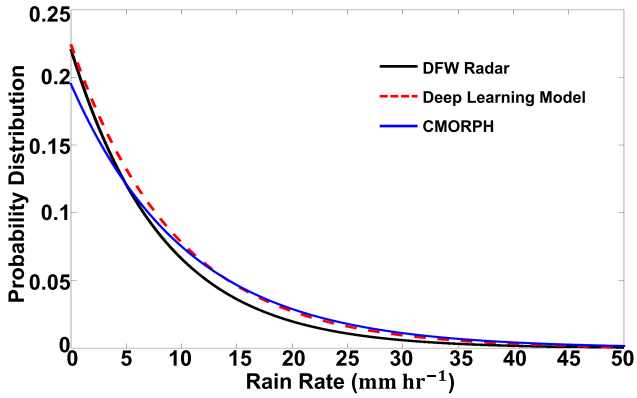

Fig. 11. Probability distribution of the estimated rain rates from the ground-based DFW radar network, the proposed deep learning model, and the standard CMORPH system for two testing events listed in Table I.

IV. SUMMARY AND FUTURE WORK

Due to the limited space–time sampling frequencies of satellite sensors, it is impossible to produce global precipitation measurements using single-source data [56]. Previous studies have attempted to combine multi-sourced satellite and rain gauge data to create spatially complete precipitation products at the global scale. A typical example is the CMORPH product developed by the NOAA's CPC, which combines the existing LEO satellite PMW-based retrievals and GEO satellite IR brightness temperature information [8], [9]. The space-based precipitation products are commonly verified using the ground radar-derived precipitation estimates [57]. In fact, ground radar

networks are still the main sources for regional and continental weather applications. Since the introduction of the dual-polarization concept [19], [58], tremendous progress has been made in the field of polarimetric radar systems and rainfall methodologies. The modern dual-polarization radar offers a number of advantages over a traditional single-polarization radar in characterizing precipitation microphysics and particle size distributions. It is also a powerful tool to discriminate precipitation echoes from nonprecipitation echoes, such as ground clutter. In addition, the National Science Foundation (NSF) Center for CASA has demonstrated that weather sensing in the lower atmosphere can be further enhanced by deploying dual-polarization, short-wavelength radar networks.

This article has introduced an innovative machine learning framework for remote sensing precipitation estimation. In particular, a deep learning MLP model is designed to produce rainfall estimates using satellite IR data and PMW-based retrievals as inputs and the ground radar network-based estimates as target labels in the training of this MLP model. An initial experiment has been conducted to verify the feasibility of this data fusion system using the satellite and CASA radar network observations in DFW metroplex. Although more case studies and extensive evaluation over different climate regions should be performed in the future, the preliminary results based on the MLP model are quite promising. The main points are summarized as follows.

1) Although the CMORPH input data sources are used in the demonstration study, the deep learning framework is designed with high flexibility. It is capable of involving different radar and satellite data sources. Such flexibility provides an efficient way to include new satellite sensors to the system and apply this data fusion system in any other regions where ground radar data are available.
2) The CMORPH rain mapping technique has been employed to combine data from individual satellites to common latitude/longitude grids before ingesting them in the proposed deep learning model. This is also for the purpose of using the standard CMORPH products to cross-validate the feasibility of the designed model.
3) The urban scale demonstration study over the DFW area demonstrates the applicability of the proposed data fusion framework. Overall, it can capture the precipitation pattern and intensity fairly well compared with ground radar-based estimates and the standard CMORPH products. For the two validation cases presented in this article, this nonparametric machine learning approach can capture low rain rates, which is slightly better than CMORPH.
4) When the PMW-based retrievals are not available for a given time and location, the proposed MLP model can still generate reasonable precipitation estimates using PMW retrievals from the nearby time periods. Compared with CMORPH that uses cloud motion vectors derived from the IR data to propagate the PMW-based retrievals, the nonparametric system developed in this article can be used as an alternative tool for dealing with incomplete PMW sensor observations.

Nevertheless, it should be pointed out that although the results in this demonstration study are quite promising, a lot of work still needs to be done before using this approach to produce routine operational products. From an engineering perspective, the high-quality high-resolution radar data used in this study are only available over the DFW metroplex. As such, the designed MLP model is trained only using local observations in the DFW area. Generic applications of this locally trained model in other regions are still under investigation. In addition, if additional radars are available in other implementation regions (e.g., regions covered by NEXRAD), the designed data fusion system can be enhanced with auxiliary radar data, that is, the model should be retrained to include new radar and satellite data that can better represent local precipitation microphysics. For regions not covered by any weather radars (e.g., oceans), we expect that this model can still be applied to the satellite observations, provided that the model is trained with ample data representing different climatological properties. From the scientific perspective, the precipitation events over the DFW area are mostly characterized by convective rain. As a result, the trained model may not be sufficient to represent other precipitation regimes dominated by stratiform rain. In addition, the temporally averaged radar data over a half-hour window may not be sufficient to represent precipitation distributions at any instant within this 30-min period. This information will be included along with the second generation of CMORPH products [9]. The target labels (i.e., mean radar estimates over 30 min) will then need to be replaced with matched instantaneous radar-based measurements. Furthermore, diurnal cycle and seasonal variability of precipitation are not considered in this article. Future research should improve all these aspects.

ACKNOWLEDGMENT

The authors would like to thank J. L. Bytheway (NOAA/ESRL and CU/CIRES) and four anonymous external reviewers for providing careful review and comments on this article. The North Central Texas Council of Governments (NCTCOG) and the National Weather Service (NWS) provided support for the operation of the Dallas–Fort Worth (DFW) urban radar network.

REFERENCES

[1] C. Kidd *et al.*, "So, how much of the earth's surface is covered by rain gauges?" *Bull. Amer. Meteorolog. Soc.*, vol. 98, pp. 69–78, Jan. 2017.
[2] K.-I. Hsu, X. Gao, S. Sorooshian, and H. V. Gupta, "Precipitation estimation from remotely sensed information using artificial neural networks," *J. Appl. Meteorol.*, vol. 36, no. 9, pp. 1176–1190, 1997.
[3] S. Sorooshian, K.-L. Hsu, X. Gao, H. V. Gupta, B. Imam, and D. Braithwaite, "Evaluation of PERSIANN system satellite-based estimates of tropical rainfall," *Bull. Amer. Meteorolog. Soc.*, vol. 81, no. 9, pp. 2035–2046, Sep. 2000.
[4] Y. Hong, K.-L. Hsu, S. Sorooshian, and X. Gao, "Precipitation estimation from remotely sensed imagery using an artificial neural network cloud classification system," *J. Appl. Meteorol.*, vol. 43, no. 12, pp. 1834–1853, 2004.
[5] G. J. Huffman, D. T. Bolvin, E. J. Nelkin, and D. B. Wolff, "The TRMM multisatellite precipitation analysis (TMPA): Quasi-global, multiyear, combined-sensor precipitation estimates at fine scales," *J. Hydrometeorol.*, vol. 8, no. 1, pp. 38–55, Feb. 2007.

[6] T. Kubota *et al.*, "Global precipitation map using satellite-borne microwave radiometers by the GSMaP project: Production and validation," *IEEE Trans. Geosci. Remote Sens.*, vol. 45, no. 7, pp. 2259–2275, Jul. 2007.

[7] T. Ushio *et al.*, "A Kalman filter approach to the global satellite mapping of precipitation (GSMaP) from combined passive microwave and infrared radiometric data," *J. Meteorolog. Soc. Japan. II*, vol. 87A, pp. 137–151, Aug. 2009.

[8] R. J. Joyce, J. E. Janowiak, P. A. Arkin, and P. Xie, "CMORPH: A method that produces global precipitation estimates from passive microwave and infrared data at high spatial and temporal resolution," *J. Hydrometeorol.*, vol. 5, no. 3, pp. 487–503, Jun. 2004.

[9] P. Xie *et al.*, "Reprocessed, bias-corrected CMORPH global high-resolution precipitation estimates from 1998," *J. Hydrometeorol.*, vol. 18, pp. 1617–1641, Jun. 2017.

[10] G. J. Huffman *et al.*, *NASA Global Precipitation Measurement (GPM) Integrated Multi-Satellite Retrievals For GPM (IMERG), Version 5.2*, document, ATBD, Greenbelt, Maryland, 2018, pp. 1–35.

[11] P. Xie and P. A. Arkin, "Global precipitation: A 17-year monthly analysis based on gauge observations, satellite estimates, and numerical model outputs," *Bull. Amer. Meteorolog. Soc.*, vol. 78, pp. 2539–2558, Nov. 1997.

[12] E. E. Ebert, J. E. Janowiak, and C. Kidd, "Comparison of near-real-time precipitation estimates from satellite observations and numerical models," *Bull. Amer. Meteorolog. Soc.*, vol. 88, pp. 47–64, Jan. 2007.

[13] G. A. Vicente, R. A. Scofield, and W. P. Menzel, "The operational GOES infrared rainfall estimation technique," *Bull. Amer. Meteorolog. Soc.*, vol. 79, no. 9, pp. 1883–1898, 1998.

[14] C. Kidd, D. R. Kniveton, M. C. Todd, and T. J. Bellerby, "Satellite rainfall estimation using combined passive microwave and infrared algorithms," *J. Hydrometeorol.*, vol. 4, pp. 1088–1104, Dec. 2003.

[15] C. Kummerow *et al.*, "The evolution of the Goddard profiling algorithm (GPROF) for rainfall estimation from passive microwave sensors," *J. Appl. Meteorol.*, vol. 40, no. 11, pp. 1801–1820, 2001.

[16] R. R. Ferraro *et al.*, "NOAA operational hydrological products derived from the advanced microwave sounding unit," *IEEE Trans. Geosci. Remote Sens.*, vol. 43, no. 5, pp. 1036–1049, May 2005.

[17] A. Behrangi and Y. Wen, "On the spatial and temporal sampling errors of remotely sensed precipitation products," *Remote Sens.*, vol. 9, no. 11, p. 1127, 2017.

[18] G. Tang, D. Long, Y. Hong, J. Gao, and W. Wan, "Documentation of multifactorial relationships between precipitation and topography of the Tibetan Plateau using spaceborne precipitation radars," *Remote Sens. Environ.*, vol. 208, pp. 82–96, Apr. 2018.

[19] V. N. Bringi and V. Chandrasekar, *Polarimetric Doppler Weather Radar: Principles and Applications*. Cambridge, U.K.: Cambridge Univ. Press, 2001.

[20] R. Cifelli, W. A. Petersen, L. D. Carey, S. A. Rutledge, and M. A. da Silva Dias, "Radar observations of the kinematic, microphysical, and precipitation characteristics of two MCSs in TRMM LBA," *J. Geophys. Res.*, vol. 107, pp. LBA 44-1–LBA 44-16, Oct. 2002.

[21] H. Chen, V. Chandrasekar, and R. Bechini, "An improved dual-polarization radar rainfall algorithm (DROPS2.0): Application in NASA IFloodS field campaign," *J. Hydrometeorol.*, vol. 18, no. 4, pp. 917–937, 2017.

[22] S. Y. Matrosov, "X-band polarimetric radar measurements of rainfall," *Amer. Meteorolog. Soc.*, vol. 41, pp. 941–952, Sep. 2002.

[23] D. McLaughlin *et al.*, "Short-wavelength technology and the potential for distributed networks of small radar systems," *Bull. Amer. Meteorolog. Soc.*, vol. 90, pp. 1797–1818, Dec. 2009.

[24] V. Chandrasekar, H. Chen, and B. Philips, "Principles of high-resolution radar network for hazard mitigation and disaster management in an urban environment," *J. Meteorolog. Soc. Jpn.*, vol. 96, pp. 119–139, Jan. 2018.

[25] R. Cifelli, V. Chandrasekar, H. Chen, and L. E. Johnson, "High resolution radar quantitative precipitation estimation in the San Francisco Bay Area: Rainfall monitoring for the urban environment," *J. Meteorolog. Soc. Jpn.*, vol. 96A, pp. 141–155, May 2018.

[26] H. Chen and V. Chandrasekar, "The quantitative precipitation estimation system for Dallas–Fort Worth (DFW) urban remote sensing network," *J. Hydrol.*, vol. 531, pp. 259–271, Dec. 2015.

[27] S. Thorndahl *et al.*, "Weather radar rainfall data in urban hydrology," *Hydrol. Earth Syst. Sci.*, vol. 21, no. 3, pp. 1359–1380, 2017.

[28] V. Chandrasekar, Y. Wang, and H. Chen, "The CASA quantitative precipitation estimation system: A five year validation study," *Natural Hazards Earth Syst. Sci.*, vol. 12, pp. 2811–2820, Sep. 2012.

[29] H. Chen and V. Chandrasekar, "Real-time wind velocity retrieval in the precipitation system using high-resolution operational multi-radar network," in *Remote Sensing of Aerosols, Clouds, and Precipitation*, T. Islam, Y. Hu, A. Kokhanovsky, and J. Wang, Eds. Amsterdam, The Netherlands: Elsevier, 2018, pp. 315–339.

[30] Y. Wen, A. Behrangi, B. Lambrigtsen, and P.-E. Kirstetter, "Evaluation and uncertainty estimation of the latest radar and satellite snowfall products using SNOTEL measurements over mountainous regions in western United States," *Remote Sens.*, vol. 8, no. 11, p. 904, 2016.

[31] S. J. Munchak and G. Skofronick-Jackson, "Evaluation of precipitation detection over various surfaces from passive microwave imagers and sounders," *Atmos. Res.*, vol. 131, pp. 81–94, Sep. 2013.

[32] H. Chen and V. Chandrasekar, "Validation of NASA's global precipitation measurement mission with a high-resolution ground radar network," in *Proc. URSI Asia–Pacific Radio Sci. Conf. (URSI AP-RASC)*, Aug. 2016, pp. 836–839.

[33] V. Chandrasekar, H. Chen, and W. Petersen, "Error and uncertainty quantification in precipitation retrievals from GPM/DPR using ground-based dual-polarization radar observations," in *Proc. EGU Gen. Assem. (EGU)*, Vienna, Austria, Apr. 2017, pp. 23–28.

[34] Y. Derin *et al.*, "Passive microwave rainfall error analysis using high-resolution X-band dual-polarization radar observations in complex terrain," *IEEE Trans. Geosci. Remote Sens.*, vol. 56, no. 5, pp. 2565–2586, May 2018.

[35] A. Gingrey, A. Varble, and E. Zipser, "Relationships between extreme rain rates and convective intensities from the perspectives of TRMM and WSR-88D radars," *J. Appl. Meteorol. Climatol.*, vol. 57, pp. 1353–1369, Jun. 2018.

[36] Y. Wen *et al.*, "Cross validation of spaceborne radar and ground polarimetric radar aided by polarimetric echo classification of hydrometeor types," *J. Appl. Meteorol. Climatol.*, vol. 50, no. 7, pp. 1389–1402, 2011.

[37] P. Kirstetter *et al.*, "Toward a framework for systematic error modeling of spaceborne precipitation radar with NOAA/NSSL ground radar–based national Mosaic QPE," *J. Hydrometeorol.*, vol. 13, pp. 1285–1300, Aug. 2012.

[38] S. Chen *et al.*, "Intercomparison of Precipitation Estimates From WSR-88D Radar and TRMM Measurement Over Continental United States," *IEEE Trans. Geosci. Remote Sens.*, vol. 53, no. 8, pp. 4444–4456, Aug. 2015.

[39] R. J. Kuligowski, Y. Li, Y. Hao, and Y. Zhang, "Improvements to the GOES-R rainfall rate algorithm," *J. Hydrometeorol.*, vol. 17, pp. 1693–1704, Jun. 2016.

[40] Y. LeCun, Y. Bengio, and G. Hinton, "Deep learning," *Nature*, vol. 521, pp. 436–444, May 2015.

[41] W. S. McCulloch and W. Pitts, "A logical calculus of ideas immanent in nervous activity," *Bull. Math. Biophys.*, vol. 5, no. 4, pp. 115–133, Dec. 1943.

[42] R. H. R. Hahnloser, R. Sarpeshkar, M. A. Mahowald, R. J. Douglas, and H. S. Seung, "Digital selection and analogue amplification coexist in a cortex-inspired silicon circuit," *Nature*, vol. 405, no. 6789, pp. 947–951, Jun. 2000.

[43] V. Nair and G. E. Hinton, "Rectified linear units improve restricted Boltzmann machines," in *Proc. 27th Int. Conf. Int. Conf. Mach. Learn.*, Jun. 2010, pp. 807–814.

[44] P. Ramachandran, B. Zoph, and Q. V. Le, "Searching for activation functions," *CoRR*, pp. 1–13, Oct. 2017. [Online]. Available: http://arxiv.org/abs/1710.05941

[45] C. Burges *et al.*, "Learning to rank using gradient descent," in *Proc. 22nd Int. Conf. Mach. Learn. (ICML)*, Aug. 2005, pp. 89–96.

[46] Y. Bengio, "Practical recommendations for gradient-based training of deep architectures," in *Neural Networks: Tricks of the Trade*. Berlin, Germany: Springer, 2012, pp. 437–478.

[47] R. Cifelli, V. Chandrasekar, S. Lim, P. C. Kennedy, Y. Wang, and S. A. Rutledge, "A new dual-polarization radar rainfall algorithm: Application in Colorado precipitation events," *J. Atmos. Ocean. Technol.*, vol. 28, pp. 352–364, Mar. 2011.

[48] R. Bechini and V. Chandrasekar, "A semisupervised robust hydrometeor classification method for dual-polarization radar applications," *J. Atmos. Ocean. Technol.*, vol. 32, pp. 22–47, Jan. 2015.

[49] Y. Wen *et al.*, "Incorporating NASA spaceborne radar data into NOAA national mosaic QPE system for improved precipitation measurement: A physically based VPR identification and enhancement method," *J. Hydrometeorol.*, vol. 14, no. 4, pp. 1293–1307, 2013.

[50] A. V. Ryzhkov, S. E. Giangrande, and T. J. Schuur, "Rainfall estimation with a polarimetric prototype of WSR-88D," *J. Appl. Meteorol.*, vol. 44, pp. 502–515, Apr. 2005.

[51] J. Zhang *et al.*, "National Mosaic and multi-sensor QPE (NMQ) system: Description, results, and future plans," *Bull. Amer. Meteorolog. Soc.*, vol. 92, pp. 1321–1338, Oct. 2011.
[52] Y. Wen *et al.*, "Evaluation of a method to enhance real-time, ground radar–based rainfall estimates using climatological profiles of reflectivity from space," *J. Hydrometeorol.*, vol. 17, no. 3, pp. 761–775, 2016.
[53] A. Rafieeinasab *et al.*, "Toward high-resolution flash flood prediction in large urban areas–Analysis of sensitivity to spatiotemporal resolution of rainfall input and hydrologic modeling," *J. Hydrol.*, vol. 531, no. 2, pp. 370–388, 2015.
[54] C. Guilloteau, E. Foufoula-Georgiou, and C. D. Kummerow, "Global multiscale evaluation of satellite passive microwave retrieval of precipitation during the TRMM and GPM eras: Effective resolution and regional diagnostics for future algorithm development," *J. Hydrometeorol.*, vol. 18, pp. 3051–3070, Nov. 2017.
[55] J. E. Janowiak, R. J. Joyce, and Y. Yarosh, "A real-time global half-hourly pixel-resolution infrared dataset and its applications," *Bull. Amer. Meteorolog. Soc.*, vol. 82, pp. 205–217, Feb. 2001.
[56] S. Michaelides, V. Levizzani, E. Anagnostou, P. Bauer, T. Kasparis, and J. E. Lane, "Precipitation: Measurement, remote sensing, climatology and modeling," *Atmos. Res.*, vol. 94, pp. 512–533, Dec. 2009.
[57] H. Chen, V. Chandrasekar, H. Tan, and R. Cifelli, "Rainfall estimation from ground radar and TRMM precipitation radar using hybrid deep neural networks," *Geophys. Res. Lett.*, to be published. doi: 10.1029/2019GL084771.
[58] T. A. Seliga and V. N. Bringi, "Potential use of radar differential reflectivity measurements at orthogonal polarizations for measuring precipitation," *J. Appl. Meteorol.*, vol. 15, pp. 69–76, Jan. 1976.

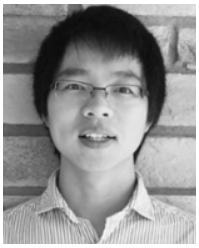

Haonan Chen (S'08–M'17) received the bachelor's degree from the Chongqing University of Posts and Telecommunications, Chongqing, China, in 2010, and the M.S. and Ph.D. degrees from Colorado State University (CSU), Fort Collins, CO, USA, in 2013 and 2017, respectively, all in electrical engineering.

He has been with the Physical Sciences Division, NOAA's Earth System Research Laboratory, Boulder, CO, USA, since 2012, first as a Research Student and then as a National Research Council (NRC) Research Associate, where he is currently a Radar, Satellite, and Precipitation Scientist with the Cooperative Institute for Research in the Atmosphere (CIRA), CSU. He is also an Affiliate Faculty Member with the Department of Electrical and Computer Engineering, CSU. He specializes in radar systems and networking, precipitation classification and estimation with polarimetric radar measurements, and multiscale radar and satellite data fusion. His research interests include the understanding of the physical sciences in the hydrometeorological processes through remote sensing technologies.

Dr. Chen serves as an Associate Editor for the *Journal of Atmospheric and Oceanic Technology* and *URSI Radio Science Bulletin* and a Guest Editor for *Remote Sensing*.

V. Chandrasekar (S'83–M'87–F'03) received the bachelor's degree from IIT Kharagpur, Kharagpur, India, and the Ph.D. degree from Colorado State University (CSU), Fort Collins, CO, USA.

He has been a Visiting Professor with the National Research Council of Italy, Rome, Italy, the University of Helsinki, Helsinki, Finland, the Finnish Meteorological Institute, Helsinki, Tsinghua University, Beijing, China, and IIT Kharagpur, an Affiliate Scientist with the National Aeronautics and Space Administration (NASA)'s Jet Propulsion Laboratory, Pasadena, CA, USA, a Distinguished Visiting Scientist with the NASA Goddard Space Flight Center, Greenbelt, MD, USA, and a Distinguished Professor of Finland (FiDiPro). He has also been a Director of the Research Experiences for Undergraduate Program for over 25 years, where he is involved in promoting research in the undergraduate curriculum. He is currently a University Distinguished Professor with CSU. He is also the Research Director of the National Science Foundation Engineering Research Center for Collaborative Adaptive Sensing of the Atmosphere. He is also the Associate Dean of the College of Engineering for promoting international research collaboration. He has been actively involved in the research and development of weather radar systems for over 35 years. He has played a key role in developing the CSU-CHILL National Radar Facility as one of the most advanced meteorological radar systems available for research and continues to work actively with the CSU-CHILL radar, supporting its research and education mission. He is an avid experimentalist conducting special experiments to collect *in situ* observations to verify the new techniques and technologies. He has served as an Academic Advisor for over 70 graduate students. He has authored two textbooks and five general books and over 250 peer-reviewed journal articles.

Dr. Chandrasekar has served as a member of the National Academy of Sciences Committee that wrote the books *Weather Radar Technology Beyond NEXRAD* and *Flash Flood Forecasting in Complex Terrain*. He is a fellow of the American Meteorological Society, the International Union of Radio Science (URSI), and the National Oceanic and Atmospheric Administration (NOAA) Cooperative Institute for Research in the Atmosphere (CIRA). He was a recipient of numerous awards, including Knighted by the Government of Finland, the NASA Technical Contribution Award, NASA Group Achievement Award, the NASA Robert H. Goddard Exceptional Achievement Award, the Outstanding Advisor Award, the CSU Innovations Award, the IEEE GRSS Education Award, the NOAA/NWS Directors Medal of Excellence, and the IEEE GRSS Distinguished Achievement Award. He has served as the General Chair for the IEEE International Geoscience and Remote Sensing Symposium (IGARSS 2006). He serves as the Chair for URSI (Commission F). He also served as the Chief Editor for the *Journal of Atmospheric and Oceanic Technology* and a Guest Editor for the IEEE TRANSACTIONS ON GEOSCIENCE AND REMOTE SENSING and the IEEE JOURNAL OF SELECTED TOPICS IN APPLIED EARTH OBSERVATIONS AND REMOTE SENSING.

Robert Cifelli received the bachelor's degree in geology from the University of Colorado at Boulder, Boulder, CO, USA, in 1983, the M.S. degree in hydrogeology from West Virginia University, Morgantown, WV, USA, in 1986, and the Ph.D. degree in atmospheric science from Colorado State University, Fort Collins, CO, USA, in 1996.

He is a radar meteorologist with over 25 years of experience in precipitation research. Since 2009, he has led the National Oceanic and Atmospheric Administration (NOAA) scientists dedicated to improving precipitation and hydrologic prediction in complex terrain and other geographic regions. He currently leads the Hydrometeorology Modeling and Applications (HMA) Team, the Physical Sciences Division, NOAA's Earth System Research Laboratory, Boulder. He also works closely with the NOAA Office of Water Prediction (OWP) on the evaluation of forcing for hydrologic prediction, physical process representation in the National Water Model, and coordination of QPE and forecast efforts across NOAA to address internal OWP and external stakeholder needs. A major focus of HMA is to improve the understanding of physical processes represented in the National Water Model and to guide future model development. He continues to work closely with the Reclamation Research and Development Office on developing improved weather, climate, and water forecasts of extreme events to better meet water management needs. He has over 50 publications in peer-reviewed journal articles.

Dr. Cifelli completed a detail with the Bureau of Reclamation through the President's Management Council Interagency Rotation Program in 2016.

Pingping Xie, photograph and biography not available at the time of publication